Location and Topology of the Fundamental Gap in Photonic Crystals

Thomas Christensen,[1,*] Hoi Chun Po,[1,2] John D. Joannopoulos,[1] and Marin Soljačić[1]
[1]Department of Physics, Massachusetts Institute of Technology, Cambridge, Massachusetts 02139, USA
[2]Department of Physics, Hong Kong University of Science and Technology, Clear Water Bay, Hong Kong, China

(Received 9 July 2021; accepted 3 May 2022; published 27 June 2022)

The fundamental, or first, band gap is of unmatched importance in the study of photonic crystals. Here, we address precisely where this gap can be opened in the band structure of three-dimensional photonic crystals. Although strongly constrained by symmetry, this problem cannot be addressed directly with conventional band-symmetry analysis due to the existence of a photonic polarization vortex at zero frequency. We develop an approach for overcoming the associated symmetry singularity by incorporating fictitious, auxiliary longitudinal modes. Our strategy also enables us to extend recent developments in symmetry-based topological analysis to the fundamental gap of three-dimensional photonic crystals. Exploiting this, we systematically study the topology of the minimal fundamental gaps. This reveals the existence of topological gap obstructions that push the fundamental gap higher than what a conventional analysis would suggest. Our work demonstrates that topology can play a crucial role in the opening of the fundamental photonic gap and informs future theoretical and experimental searches for conventional and topological band gaps in three-dimensional photonic crystals.

DOI: 10.1103/PhysRevX.12.021066

Subject Areas: Condensed Matter Physics
Photonics, Topological Insulators

I. INTRODUCTION

The pursuit of photonic band gaps has been a key driving force in the field of photonic crystals (PhCs) [1,2], from Rayleigh's earliest treatments of one-dimensional PhCs in 1887 [3,4], to Yablonovitch's [5] and John's [6] three-dimensional (3D) generalizations a century later, and continuing to this day [7,8]. The recent incorporation of ideas from topological band theory [9–11] to photonics [12–14] has reinvigorated this fascination by highlighting that PhC bands—and the gaps between them—can possess robust topological properties. Armed with recent insights from topological band theory, we address one of the fundamental problems in the study of 3D PhCs: Where is the lowest photonic band gap in the band structure, and what is its topology?

In more precise terms, we ask how many bands are required, at minimum, by spatial and time-reversal (TR) symmetry below the first photonic gap [Fig. 1(a)], i.e., where it can be opened. The first, or fundamental, gap is special—and of particular interest—for two reasons: (1) The first photonic gap is usually the largest and most easily engineered [15], and (2) the bands below the first gap in a PhC are unlike all other bosonic quasiparticle bands because they connect to a polarization singularity at zero frequency ($\omega = 0$) and zero momentum ($\mathbf{k} = \mathbf{0}$, i.e., Γ). This singularity arises because of the transverse polarization of photons [Fig. 1(b)] and has profound implications for the first gap: In general, the number of bands required below the first gap is different from that required between higher-lying gaps since the latter are not affected by the singularity [16–18]. The singularity additionally renders the band symmetry at Γ ill-defined, ostensibly preventing application of symmetry-based topological analysis to the most important gap of 3D PhCs [19].

A systematic study of this minimum-connectivity problem for PhCs was recently initiated by Watanabe and Lu [16], who derived various lower bounds for the number of connected bands using sub- and supergroup relations. Given a specific PhC, however, it is unclear, in general, if these lower bounds have already made maximal use of the present spatial symmetries. In addition, the topology of the bands below the first gap remains unaddressed.

Here, we develop new tools that enable us to establish the exact minimum connectivity and topology below the first gap for PhCs in each of the 230 possible symmetry settings, i.e., space groups. Our approach extends recent symmetry-based tools for topological band analysis in condensed-matter systems [20–22] to the fundamental gap of 3D PhCs, overcoming the apparent barrier raised by the singular Γ-point symmetry. Surprisingly, we find

*tchr@mit.edu

Published by the American Physical Society under the terms of the Creative Commons Attribution 4.0 International license. Further distribution of this work must maintain attribution to the author(s) and the published article's title, journal citation, and DOI.

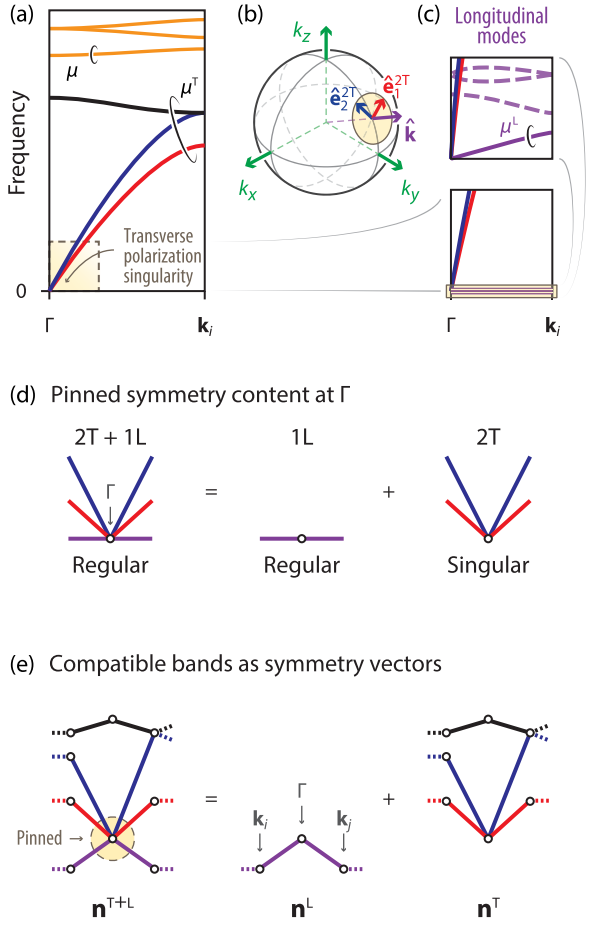

FIG. 1. PhC band connectivity below the fundamental gap. (a) The two lowest-frequency "lightlike" PhC bands (blue and red) are pinned to $\omega = 0$ at the Γ point. The minimum connectivity μ^T of these bands, i.e., below the fundamental gap, is generally not equal to the minimum connectivity μ of higher bands (orange). (b) The polarization vectors $\hat{\mathbf{e}}_{1,2}^{2T}$ of the transverse modes near $\omega = 0$ span a space (yellow disk) that varies with wave-vector orientation $\hat{\mathbf{k}}$, rendering their associated symmetry content at Γ singular. (c) In addition to physical, transverse PhC modes, the Maxwell equations also admit a set of nonphysical, longitudinal modes (purple). (d) The singularity can be regularized by adding a longitudinal mode (1L) to the two transverse modes (2T) at $\omega = 0$. (e) Realizable band configurations connected to $\omega = 0$ correspond to compatibility-allowed symmetry vectors $\mathbf{n}^{T+L}$ of the combined transverse and longitudinal band set, which is itself a sum of longitudinal and transverse contributions $\mathbf{n}^L$ and $\mathbf{n}^T$.

that complete answers to the photonic minimum-connectivity question cannot be obtained without topological considerations. Specifically, we find six space groups whose minimum-connectivity bands are all topologically nontrivial, entailing a topological obstruction to the opening of the symmetry-allowed gap. This effect, which we term "Γ-enforced topology," resembles filling-enforced topology [23,24] but arises here as a direct consequence of the zero-frequency Γ-point singularity. For PhCs with Γ-enforced topology, observing a minimum-connectivity fundamental gap along the high-symmetry lines implies that the gap must close at nodal lines in the interior of the Brillouin zone (BZ). This pushes the true fundamental gap to the higher-energy part of the spectrum—an insight from topological band theory that cannot be inferred from conventional symmetry analysis alone. Finally, as the analogous minimum-connectivity problem for *phonons* occurs as a subproblem in our approach, we solve the phononic problem as well.

II. THEORETICAL FRAMEWORK

The two lowest-frequency transverse (2T) solutions of nonmetallic PhCs (i.e., with periodic and non-negative dielectric ε and magnetic μ response) asymptotically realize the effective-medium approximation at small momenta $|\mathbf{k}| \to 0$, where they touch $\omega = 0$ with the lightlike linear dispersion $(\overline{\varepsilon^{-1}\mu^{-1}})^{1/2}c|\mathbf{k}|$ [Fig. 1(a)]. Their displacement fields converge to plane waves $\mathbf{D}_{\sigma\mathbf{k}}^{2T}(\mathbf{r}) \sim \hat{\mathbf{e}}_{\sigma\mathbf{k}}^{2T}e^{i\mathbf{k}\cdot\mathbf{r}}$ ($\sigma = 1, 2$), with mutually orthogonal polarization vectors $\hat{\mathbf{e}}_{\sigma\mathbf{k}}^{2T}$ polarized transversely to the wave vector $\mathbf{k}$. The resulting vortexlike polarization texture around the Γ point [Fig. 1(b)] renders the continuation of the 2T solutions to $|\mathbf{k}| = 0$ ill-defined (it depends on $\hat{\mathbf{k}}$) and is the salient feature that distinguishes photons from all other bosonic quasiparticles (e.g., phonons, excitons, or magnons) in the present context.

The above considerations show that the lightlike 2T modes behave as free photons (in an effective medium) at small momenta. As we go to higher momenta, however, the effects of the PhC become apparent. The periodicity of the PhC leads to BZ folding, and photonic band gaps arise when energetically intersecting bands anticross with each other. Such anticrossing is heavily constrained by the spatial symmetries of the PhC since the hybridization matrix elements between bands with distinct symmetry characters vanish. Importantly, symmetry eigenvalues of rotations and mirrors as well as their nonsymmorphic counterparts—screw and glides—are continuously defined over lines and planes in the BZ. For the lowest-lying states, these symmetry eigenvalues of the bands can be traced down to the singularity at the zero-frequency limit [16]. This leads to a dilemma in the symmetry analysis of the fundamental photonic band gap: While the symmetry characters of the lowest bands are dictated by those of the lowest-lying lightlike modes, their symmetry eigenvalues are ill-defined in the zero-momentum limit.

In the following, we outline our theoretical framework and strategy for overcoming the singularity problem. We first describe the fundamental relationship between band connectivity, compatibility relations, and band symmetries and introduce a scheme to generate all allowable band symmetries through stacking of a minimal set of intrinsically connected bands (Sec. II A). We then discuss the implications of the polarization vortex in the context of

pinned symmetry and compatibility relations (Sec. II B) and introduce a regularization strategy featuring auxiliary apolar and longitudinal modes (Sec. II C). Following this overview, Sec. III considers the results obtained from the application of our theoretical framework. The results for the minimum photonic connectivity below the first gap are given first (Sec. III A). Next, we introduce a scheme to evaluate the symmetry-identifiable topology of the otherwise singular photonic bands below the first gap and use it to determine the topology of all minimum-connectivity solutions (Sec. III B). Our analysis uncovers six space groups whose minimum-connectivity solutions are all topologically nontrivial and consequently display a topological obstruction to gap opening. We end by introducing two concrete PhCs that demonstrate this effect (Sec. III C).

A. Compatibility relations and band connectivity

The presence of crystalline symmetries constrains the possible connections between energy bands across the BZ due to the existence of compatibility relations [25–28]. These relations express a familiar notion, namely, the splitting of symmetry-protected degeneracies in finite systems but translated to $\mathbf{k}$-space. In finite systems, such degeneracies can be split only by deforming the considered object to a state of lowered symmetry (i.e., by lowering the point-group symmetry). In crystalline systems, however, the modal symmetry at any given $\mathbf{k}$-point in the band structure is determined by the subset of the space-group symmetry that additionally leaves the considered $\mathbf{k}$-point invariant (i.e., by the little group of $\mathbf{k}$). Compatibility relations express how modal degeneracy and symmetry are reduced or maintained as we move off an initial high-symmetry point towards a lower-symmetry line (or plane). Since such lines can connect to other high-symmetry $\mathbf{k}$-points—e.g., starting at Γ and moving towards k_x, one reaches the high-symmetry point X at the BZ boundary—and since continuity requires modal symmetry to be invariant along lines of fixed symmetry, the compatibility relations at distinct high-symmetry points become coupled, effectively tying together multiple local relations into a global set of consistency constraints spanning the BZ. These global constraints restrict how (and how many times) bands must connect and, crucially, when they can be gapped [17,29].

For any given space group, the solutions to the aggregate set of compatibility constraints (along with a requirement that all symmetry data be non-negative) define the set of all physically realizable band structures $\{\mathrm{BS}\}$. Each element of $\{\mathrm{BS}\}$ can be identified with a "symmetry vector" $\mathbf{n}$ that enumerates the symmetry content of the included bands across all nonequivalent $\mathbf{k}$-points, $\{\mathbf{k}_i\}$, in the BZ. The elements of $\mathbf{n}$ give the multiplicity $n^\alpha_{\mathbf{k}_i}$ of the αth small irreducible representation (irrep) $D^\alpha_{\mathbf{k}_i}$ in the little group $G_{\mathbf{k}_i}$ at $\mathbf{k}_i$ [30], such that

$$\mathbf{n} \equiv [n^1_{\mathbf{k}_1}, n^2_{\mathbf{k}_1}, \ldots, n^1_{\mathbf{k}_i}, n^2_{\mathbf{k}_i}, \ldots, \mu]^{\mathrm{T}}, \tag{1}$$

with the number of included bands μ incorporated as well. We denote by $\mathbf{n}_{\mathbf{k}} \equiv [n^1_{\mathbf{k}}, n^2_{\mathbf{k}}, \ldots]^{\mathrm{T}}$ the projection of $\mathbf{n}$ to its content at a particular $\mathbf{k}$. To obtain $\mathbf{n}_{\mathbf{k}}$ for a band grouping $\{n'\}$, we first compute the symmetry eigenvalues $x_{n\mathbf{k}}(g) \equiv \langle \mathbf{E}_{n\mathbf{k}} | g \mathbf{D}_{n\mathbf{k}} \rangle$ for each operation $g \in G_{\mathbf{k}} = \{g_1, \ldots, g_{|G_{\mathbf{k}}|}\}$ and each band $n \in \{n'\}$; next, we aggregate eigenvalues in the character vector $\mathbf{x}_{\mathbf{k}} \equiv \sum_n [x_{n\mathbf{k}}(g_1), \ldots, x_{n\mathbf{k}}(g_{|G_{\mathbf{k}}|})]^{\mathrm{T}}$; finally, we solve $\boldsymbol{\chi}_{\mathbf{k}} \mathbf{n}_{\mathbf{k}} = \mathbf{x}_{\mathbf{k}}$ for $\mathbf{n}_{\mathbf{k}}$, with $\boldsymbol{\chi}_{\mathbf{k}}$ denoting the character table of $G_{\mathbf{k}}$ with characters $\chi^\alpha_{\mathbf{k}}(g) \equiv \mathrm{Tr} D^\alpha_{\mathbf{k}}(g)$ operation-indexed (g) along rows and irrep-indexed (α) along columns. For the lossless media considered here, the associated eigenvalue problem is Hermitian under the inner product $\langle \mathbf{E}_{n\mathbf{k}} | \mathbf{D}_{n\mathbf{k}} \rangle$ [1,36]. The $\mathbf{E}$ and $\mathbf{D}$ fields transform as vector fields, i.e., $g\mathbf{D}_{n\mathbf{k}}(\mathbf{r}) = (g\mathbf{D}_{n\mathbf{k}})(g^{-1}\mathbf{r})$ [2]. Basic transformation properties of the Maxwell equations are reviewed in Sec. S1 of the Supplemental Material [37].

The structure of $\{\mathrm{BS}\}$ has been explored using both graph theory [22,38,39] and linear algebra [20,21,40]. Here, inspired by Ref. [41], we pursue a different approach that allows us to assemble $\{\mathrm{BS}\}$ from a set of minimal and intrinsically connected bands. First, we note that elements of $\{\mathrm{BS}\}$ are equipped with a composition operation, namely, "stacking" of bands (addition of symmetry vectors) but not with an analogous inverse operation (subtraction of symmetry vectors need not be physical, i.e., $\{\mathrm{BS}\}$ is not closed under subtraction). This describes the algebraic structure of a monoid: A group lacking inverse operations. More precisely, $\{\mathrm{BS}\}$ is a positive affine monoid (it is a submonoid of a free Abelian group [21], bounded by a pointed polyhedral cone) and is therefore equipped with a unique, minimal basis $\{\mathbf{h}_i\}$—a Hilbert basis [42]—whose non-negative integer combinations generate $\{\mathrm{BS}\}$:

$$\{\mathrm{BS}\} = \left\{ \sum_i c_i \mathbf{h}_i \middle| c_i \in \mathbb{N} \right\}. \tag{2}$$

As we show in Supplemental Sec. S2 [37], the basis $\{\mathbf{h}_i\}$ can be derived from a related basis, namely, the elementary band representations (EBRs) of topological quantum chemistry [22] whose stacking generates the set of all topologically trivial (or "atomic") insulators (in summary, we define $\{\mathrm{BS}\}$ as the intersection of a lattice and a polyhedral cone and obtain the associated Hilbert basis using the Normaliz software [43]). Crucially, the basis vectors $\mathbf{h}_i$ necessarily describe connected bands; otherwise, they would not form a *minimal* basis for $\{\mathrm{BS}\}$. Conceptually, the elements of $\{\mathbf{h}_i\}$ are the indivisible units whose stacking yields all separable band structures.

B. Pinned symmetry content at Γ

At first glance, the existence and properties of a Hilbert basis for $\{\mathrm{BS}\}$ would appear to solve the question of band

connectivity entirely. Indeed, denoting the connectivities associated with the Hilbert basis $\{\mathbf{h}_i\}$ by $\{\mu_i\}$, the minimum realizable connectivity of any *regular* band grouping (e.g., electrons) is just $\min\{\mu_i\}$. As noted earlier, however, photonic bands below the first gap are *not regular* due to the ill-definiteness of the 2T solutions at Γ. This ill-definiteness extends to the symmetry vector for 2T-connected bands, presenting a clear obstacle.

To overcome this, we first describe how a partial, effective assignment of the 2T Γ-point symmetry can be constructed. Specifically, we can treat the 2T Γ-point symmetry as a surrogate for compatibility constraints imposed by line and plane little groups that intersect Γ. These "interior" little groups can include proper rotations and screws r_θ (of angle θ) as well as mirrors and glides, m. Their symmetry eigenvalues can be evaluated directly from our knowledge of the asymptotic 2T fields at small $|\mathbf{k}|$ and then continued to Γ, giving $e^{\pm i\theta}$ and ± 1, respectively, as noted by Watanabe and Lu [16]. The associated characters, i.e., sum of symmetry eigenvalues, are $x_\Gamma^{2T}(r_\theta) \equiv 2\cos\theta$ and $x_\Gamma^{2T}(m) = 0$.

Unlike rotations and mirrors, improper rotations and inversions can only be symmetries at Γ or at the BZ boundary, so they are not similarly continuable to Γ. The surrogate Γ-point irrep is therefore underdetermined for space groups with (roto-)inversions. Moreover, even for the 113 space groups without (roto-)inversions, the surrogate 2T irrep can be singular. As an example, space group 16 (P222) consists of operations $\{1, 2_{001}, 2_{010}, 2_{100}\}$ and has the 2T Γ-point character vector $\mathbf{x}_\Gamma^{2T} \equiv [x_\Gamma^{2T}(1), x_\Gamma^{2T}(2_{001}), x_\Gamma^{2T}(2_{010}), x_\Gamma^{2T}(2_{100})]^T = [2,-2,-2,-2]^T$ (in CDML notation [34]). The associated Γ-projected symmetry vector is $\mathbf{n}_\Gamma^{2T} = -\Gamma_1 + \Gamma_2 + \Gamma_3 + \Gamma_4$. Notably, this includes a *subtracted* irrep Γ_1, which prevents an expansion in the Hilbert basis $\{\mathbf{h}_i\}$ (which is strictly non-negative): The 2T symmetry at Γ is singular.

We now introduce new techniques to regularize this singularity. To that end, we first observe that the Maxwell equations admit not only transverse (divergence-free) solutions but also longitudinal (curl-free) solutions, which, however, violate the transversality condition $\boldsymbol{\nabla}\cdot\mathbf{D} = \boldsymbol{\nabla}\cdot\mathbf{B} = 0$ (unless ε or μ vanishes). In local media, the longitudinal solutions are completely degenerate with eigenfrequencies $\omega_{n\mathbf{k}} = 0$. It is useful to imagine lifting their dispersion to a more conventional band structure (which, physically, can be achieved, e.g., by including nonlocality and a weak Drude term in the material response) as illustrated in Fig. 1(c). Even in this "lifted" picture, a single longitudinal solution (1L) will always connect to $\omega = 0$ at Γ with an asymptotic plane-wave-like field profile $\mathbf{D}_\mathbf{k}^{1L}(\mathbf{r}) \sim \hat{\mathbf{k}} e^{i\mathbf{k}\cdot\mathbf{r}}$. Its Γ-continuable rotation and mirror eigenvalues transform trivially, i.e., $x_\Gamma^{1L}(r_\theta) = x_\Gamma^{1L}(m) = 1$. Analogously to the 2T case, the 1L (roto-)inversion eigenvalues cannot be continued onto Γ either and appear nominally unpinned. In fact, the pinned rotation- and mirror-symmetry eigenvalues and an "emergent" O(3) effective-medium limit symmetry constrains the allowable roto-inversion eigenvalues to points in a discrete lattice (Supplemental Sec. S4 [37]). A physically natural choice among these, which we make throughout and which is possible in all space groups, is a trivially transforming 1L mode [i.e., letting $x^{1L}(g) = 1$ for *all* operations; $\mathbf{n}_\Gamma^{1L}$ is then a Γ_1 or Γ_1^+ irrep]. Thus, the Γ-symmetry content of the 1L mode can always be chosen regularly.

Further, the symmetry content of the "apolar" sum of 1L and 2T bands, i.e., $\mathbf{n}_\Gamma^{1L+2T} = \mathbf{n}_\Gamma^{1L} + \mathbf{n}_\Gamma^{2T}$, is well-defined and regular [Fig. 1(d)] because the space spanned by their combination is invariant to $\hat{\mathbf{k}}$ in the $|\mathbf{k}| \to 0$ limit. The associated characters are uniquely determined for both proper (+) and improper (−) rotations g, equaling $x_\Gamma^{1L+2T}(g) = \pm 2\cos\theta \pm 1$. Considering again space group 16, we have $\mathbf{n}_\Gamma^{1L+2T} = \Gamma_2 + \Gamma_3 + \Gamma_4$ and $\mathbf{n}_\Gamma^{1L} = \Gamma_1$, revealing that the negative Γ_1 irrep in $\mathbf{n}_\Gamma^{2T}$ simply represents a subtraction of the 1L mode. We therefore generally define the surrogate 2T symmetry at Γ as $\mathbf{n}_\Gamma^{2T} = \mathbf{n}_\Gamma^{1L+2T} - \mathbf{n}_\Gamma^{1L}$, i.e., as the subtraction of two regular representations.

C. Transverse band solutions

The Γ-symmetry content at $\omega = 0$, i.e., $\mathbf{n}_\Gamma^{1L}$, $\mathbf{n}_\Gamma^{2T}$, and $\mathbf{n}_\Gamma^{1L+2T}$, imposes constraints

$$\mathbf{n}_\Gamma^{L} \geq \mathbf{n}_\Gamma^{1L}, \qquad \mathbf{n}_\Gamma^{T} \geq \mathbf{n}_\Gamma^{2T}, \qquad \mathbf{n}_\Gamma^{L+T} \geq \mathbf{n}_\Gamma^{1L+2T}, \quad (3)$$

on the symmetry vectors of the longitudinal ($\mathbf{n}^L$), transverse ($\mathbf{n}^T$), and apolar ($\mathbf{n}^{T+L}$) band solutions connected to $\omega = 0$ [Fig. 1(e)]. These constraints, jointly with the definitions of $\mathbf{n}_\Gamma^{1L}$, $\mathbf{n}_\Gamma^{2T}$, and $\mathbf{n}_\Gamma^{1L+2T}$, fully implement the physical distinctions between the considered polarizations. We emphasize the distinctions between $\{\mathbf{n}_\Gamma^{L}, \mathbf{n}_\Gamma^{T}, \mathbf{n}_\Gamma^{L+T}\}$ and $\{\mathbf{n}_\Gamma^{1L}, \mathbf{n}_\Gamma^{2T}, \mathbf{n}_\Gamma^{1L+2T}\}$: While the former includes the Γ-symmetry content of all bands below the first gap, the latter includes only the zero-frequency content. Since $\mathbf{n}_\Gamma^{1L}$ and $\mathbf{n}_\Gamma^{1L+2T}$ are regular, the auxiliary solutions $\mathbf{n}^L$ and $\mathbf{n}^{L+T}$ can always be expanded in the Hilbert basis $\{\mathbf{h}_i\}$. However, this is generally not possible for the transverse solutions $\mathbf{n}^T$ since the constraint $\mathbf{n}_\Gamma^{2T}$ may be singular. Candidate transverse solutions can instead be obtained as the subtraction of an apolar and a longitudinal solution, i.e., as $\mathbf{n}^T = \mathbf{n}^{T+L} - \mathbf{n}^L$. Those candidates that respect the Γ constraints of Eq. (3) and are regular at all other $\mathbf{k}$-points, i.e., have

$$\mathbf{n}_{\mathbf{k}_i}^{T} \geq 0, \quad (4)$$

for all $\mathbf{k}_i \neq \Gamma$, correspond to physically realizable transverse bands connected to $\omega = 0$. If we denote by $\{\mathbf{n}^{L+T}\}$ the set of all apolar solutions and by $\tilde{\mathbf{n}}^L$ some longitudinal solution, each consistent with Eq. (3), then all transverse solutions $\{\mathbf{n}^T\}$ can be identified with the elements of the set $\{\mathbf{n}^{L+T}\} - \tilde{\mathbf{n}}^L$ that are consistent with Eqs. (3) and (4). The specific

choice of $\tilde{\mathbf{n}}^{\mathrm{L}}$ is immaterial since the transverse and auxiliary longitudinal degrees of freedom are decoupled, except at $\omega = 0$ (Supplemental Sec. S5.A [37]).

Jointly, this implies a simple strategy for determining the minimum connectivity μ^{T} below the first gap of PhCs:

1. Pick a longitudinal solution $\tilde{\mathbf{n}}^{\mathrm{L}}$ with connectivity μ^{L} and define $\mu^{\mathrm{L+T}} = \mu^{\mathrm{L}} + 2$.
2. Find all apolar solutions $\{\mathbf{n}^{\mathrm{L+T}}\}$ with connectivity $\mu^{\mathrm{L+T}}$.
3. If any $\{\mathbf{n}^{\mathrm{L+T}}\} - \tilde{\mathbf{n}}^{\mathrm{L}}$ are valid, i.e., respect Eqs. (3) and (4), they represent physically realizable transverse solutions $\{\mathbf{n}^{\mathrm{T}}\}$ with connectivity $\mu^{\mathrm{T}} = \mu^{\mathrm{L+T}} - \mu^{\mathrm{L}}$; if not, increment $\mu^{\mathrm{L+T}}$ and return to step 2.

The Hilbert basis $\{\mathbf{h}_i\}$ allows a highly efficient and exhaustive computation of the finite set of solutions in step 2 without the combinatorial challenges that a nonconical basis would present Supplemental Sec. S3.B [37]). Nonminimal connectivity solutions can be obtained by simply continuing the iteration procedure (Supplemental Sec. S8 [37]).

III. RESULTS

A. Minimum photonic band connectivity

We apply our framework to compute the minimum-connectivity transverse solutions for each of the 230 space groups [44], with and without TR symmetry [46]. As one of the central results of this work, Fig. 2 summarizes the associated minimum transverse connectivities μ^{T} versus space group. In addition to the minimum transverse connectivity, we also indicate the minimum regular connectivity μ (with TR), which applies to all bands above the first gap. As previously noted by Watanabe and Lu [16], μ^{T} is neither smaller nor larger than μ, in general: E.g., in all symmorphic space groups, the regular connectivity is $\mu = 1$, but the transverse connectivity μ^{T} is larger, equaling either 2 or 3 (at least 2 due to the double degeneracy at $\omega = 0$). Conversely, the cubic space groups 199 ($\mathrm{I2_13}$) and 214 ($\mathrm{I4_132}$; single gyroid) have $\mu^{\mathrm{T}} = 2$ *smaller* than $\mu = 4$. Reference [16] established the existence of $\mu^{\mathrm{T}} = 2$ solutions for 104 space groups and obtained $\mu^{\mathrm{T}} \geq 3$ or $\mu^{\mathrm{T}} \geq 4$ lower bounds for the remaining groups (with TR) by manually deriving compatibility-respecting solutions for 38 key groups in combination with translationengleiche [49] sub- and supergroup relations (Supplemental Sec. S6 [37]). By evaluating all solutions explicitly, we find 19 exceptions—namely, space groups 72, 114, 126, 128, 130, 133, 135, 137, 142, 169, 170, 178, 179, 218, 220, 222, 223, 228, and 230 (Fig. 2, dashed boxes)—that exceed these lower bounds (as we discuss later, accounting for topology reveals additional exceptions). The exceptions are all nonsymmorphic space groups and are associated with the presence of additional screw or glide axes—or, rarely, with inversion—relative to the considered key subgroup [50]. Generally, we observe that space groups with $\mu^{\mathrm{T}} > 2$ are either nonsymmorphic or body- or face-centered, consistently with Ref. [16]. The exact impact of nonsymmorphic symmetry is varied and detail sensitive: As an example, the nonsymmorphic tetragonal space groups 112 ($P\bar{4}2c$), 113 ($\mathrm{P\bar{4}2_1m}$), and 114 ($\mathrm{P\bar{4}2_1c}$) have μ^{T} equal to 2, 4, and 6, respectively—despite having identical point-group symmetry ($\bar{4}2\mathrm{m}$ or D_{2d}) and screws and glides that differ only in their translation parts.

We can compare our results for μ^{T} with a recent high-throughput computational search for PhC band gaps by Cersonsky *et al.* [8]. In this search, 103 space groups were identified by explicit examples as capable of hosting complete PhC gaps at a dielectric contrast below 16. In each such case, the computed number of bands below the first gap in Ref. [8] is consistent with the μ^{T} reported here (i.e., equal to or higher, with equality attained in 31 space groups) [51].

By breaking TR symmetry, e.g., via an external magnetic field, irreps that otherwise stick together because of TR are split (i.e., complex or pseudoreal irreps [47]). In 36 space groups, this leads to a reduction of the TR-broken transverse connectivity $\tilde{\mu}^{\mathrm{T}}$ relative to its TR-invariant value μ^{T} (Fig. 2, triangular cutouts). The reduction often corresponds to the splitting of a Hilbert basis vector in the TR-invariant solution into two TR-broken components that are otherwise held together by a (self-)conjugate irrep pair; e.g., in space group 161 (R3c), splitting the physically real 4D irrep T_3T_3 into two pseudoreal 2D T_3 irreps lowers $\mu^{\mathrm{T}} = 4$ to $\tilde{\mu}^{\mathrm{T}} = 2$. In these cases, applying a TR-breaking perturbation to a TR-invariant minimum-connectivity solution will necessarily lower the connectivity from μ^{T} to $\tilde{\mu}^{\mathrm{T}}$. Interestingly, several $\tilde{\mu}^{\mathrm{T}} < \mu^{\mathrm{T}}$ solutions cannot be obtained in this perturbative fashion. For instance, the TR-invariant $\mu^{\mathrm{T}} = 4$ solutions of space group 73 (Ibca) require the X-point symmetry $X_1^+ + X_2^+ + X_3^+ + X_4^+$ or $X_1^- + X_2^- + X_3^- + X_4^-$, while the TR-broken $\tilde{\mu}^{\mathrm{T}} = 2$ solution requires $X_4^+ + X_4^-$ symmetry; the latter cannot be decomposed from the former and hence also not by perturbatively breaking TR.

As in the example above, a given connectivity can usually be realized by multiple symmetry vectors $\{\mathbf{n}^{\mathrm{T}}\}$. The associated *regular* symmetry content is definite and physical—i.e., $\{\mathbf{n}_\Gamma^{\mathrm{T}}\} - \mathbf{n}_\Gamma^{\mathrm{2T}}$ and $\{\mathbf{n}_{\mathbf{k}\neq\Gamma}^{\mathrm{T}}\}$ are physical quantities—and we exhaustively enumerate every minimum-connectivity symmetry vector in Supplemental Secs. S11.A and S11.B [37]. In the following, we introduce a method to evaluate the transverse solutions' topology despite their singular Γ-point symmetry. Surprisingly, we find that topology can constrain μ^{T} beyond the requirements imposed by compatibility relations.

B. Topology of singular transverse bands

Any regular symmetry vector can be mapped to topological indices $(\nu_1, \ldots, \nu_{\lambda_{d^{\mathrm{BS}}}})$ in the symmetry indicator group $X_{\mathrm{BS}} = \mathbb{Z}_{\lambda_1} \times \ldots \times \mathbb{Z}_{\lambda_{d^{\mathrm{BS}}}}$ with $\mathbb{Z}_{\lambda_i} \equiv \{0, 1, \ldots, \lambda_i - 1\}$ (Supplemental Secs. S2.C–S2.F [37]) [21]. For brevity, we

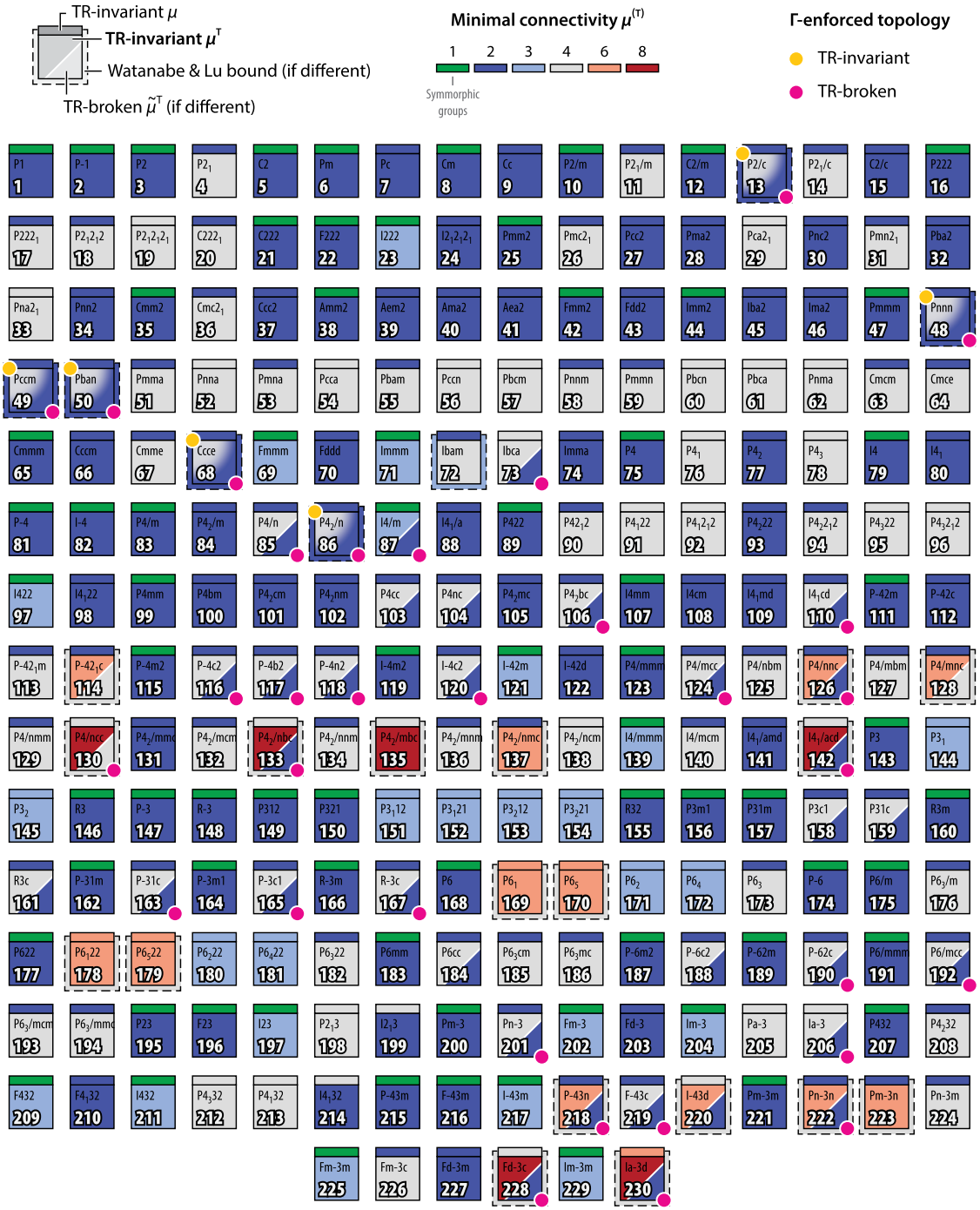

FIG. 2. Minimum photonic band connectivity and Γ-enforced topology. The TR-invariant minimum transverse band connectivity below the first gap, μ^T, is given for each space group (labeled squares). Watanabe and Lu's [16] lower bounds are shown (dashed boxes) when our explicit solutions exceed them. The corresponding TR-broken connectivities $\tilde{\mu}^T$ are shown (lower triangular cutouts) when they differ from their TR-invariant counterparts. Minimum-connectivity solutions with Γ-enforced topology are highlighted by circular markers (in yellow, with TR; in pink, without TR). TR-invariant minimum regular connectivities μ are shown as context (narrow rectangles). Compatibility relations allow $\mu^T = 2$ solutions in space groups 13, 48 – 50, 68, and 86 (lower-diagonal box shading); however, they are topologically obstructed (i.e., incompatible with a gap) because of Γ-enforced nongaps, which increases μ^T to 4 (upper-diagonal box shading).

omit trivial factor groups, i.e., write $\mathbb{Z}_{\lambda_i} \times \mathbb{Z}_1$ as $\mathbb{Z}_{\lambda_i}$ and $\mathbb{Z}_1 \times \ldots \times \mathbb{Z}_1$ as $\mathbb{Z}_1$. Space groups with symmetry-identifiable topology have indicator groups $X_{\mathrm{BS}} \neq \mathbb{Z}_1$ (equivalently, $\nu_i = 0$ denotes a trivial index): With TR symmetry, there are 53 such space groups, all corresponding to topological nodal features [52]. Denoting by **B** the

columnwise matrix concatenation of EBR vectors, and by $\mathbf{B} = \mathbf{S}\mathbf{\Lambda}\mathbf{T}$ its associated Smith normal decomposition, the topological indices of a symmetry vector $\mathbf{n} \in \{\mathrm{BS}\}$ are [53]

$$\nu_i = \mathbf{S}_{i,\star}^{-1}\mathbf{n} \bmod \lambda_i, \tag{5}$$

with $\mathbf{S}_{i,\star}^{-1}$ denoting the ith row of $\mathbf{S}^{-1}$ and λ_i the ith diagonal element of $\mathbf{\Lambda}$ (corresponding to the indicator group's $\mathbb{Z}_{\lambda_i}$ term).

For photonic bands below the first gap, a similar approach might not immediately appear workable since the associated symmetry vector $\mathbf{n}^{\mathrm{T}}$ may be singular (i.e., $\mathbf{n}^{\mathrm{T}}$ may not belong to $\{\mathrm{BS}\}$). In the spirit of K theory, we instead define indices for $\mathbf{n}^{\mathrm{T}}$ by considering the difference of the apolar ($\nu_i^{\mathrm{L+T}}$) and longitudinal (ν_i^{L}) indices, whose symmetry vectors are regular:

$$\nu_i^{\mathrm{T}} = (\nu_i^{\mathrm{L+T}} - \nu_i^{\mathrm{L}}) \bmod \lambda_i. \tag{6}$$

This is a key result of our work: It enables direct and full application of symmetry-based diagnosis for band topology to all 3D PhCs, despite the Γ-point singularity at $\omega = 0$. Crucially, while the auxiliary indices $\nu_i^{\mathrm{L+T}}$ and ν_i^{L} are not unique—Eq. (3) leaves substantial freedom of choice for the auxiliary symmetry vectors—their difference is (Supplemental Sec. S5.B [37]). In fact, since Eq. (5) is a linear relation, Eq. (6) establishes that ν_i^{T} can actually be evaluated directly from $\mathbf{n}^{\mathrm{T}}$ regardless of its singular characteristics, i.e., that $\nu_i^{\mathrm{T}} = \mathbf{S}_{i,\star}\mathbf{n}^{\mathrm{T}} \bmod \lambda_i$ [54].

C. Photonic topological nongaps

Using Eq. (6), we evaluate the symmetry-indicated topology of every minimum-connectivity transverse solution (Supplemental Secs. S11.A and S11.B [37]). In doing so, we discover six centrosymmetric and nonsymmorphic space groups—13 (P2/c), 48 (Pnnn), 49 (Pccm), 50 (Pban), 68 (Ccce), and 86 ($\mathrm{P4_2/n}$)—whose minimum-connectivity ($\mu^{\mathrm{T}} = 2$) transverse solutions are *all* topologically nontrivial (Fig. 2, yellow markers). If a gap exists between bands 2 and 3 in the high-symmetry band structure of these space groups, the resulting gap is guaranteed to be topologically nontrivial—i.e., nontrivial topology is implied by band connectivity alone. While such connectivity-implied nontriviality is reminiscent of filling-enforced topology in the electronic context [23,24], we stress that its appearance in the photonic context is intrinsically different since it is inseparable from the Γ-point singularity—accordingly, we refer to it as "Γ-enforced topology." In contrast, the minimum-connectivity solutions of TR-invariant regular bosons (e.g., photonic bands above the first gap) do not display Γ-enforced topology (Supplemental Sec. S9 [37]).

Notably, all TR-invariant, symmetry-identifiable, bosonic topology is associated with bulk nodal features: Specifically, with nodal lines and Weyl points for centrosymmetric and noncentrosymmetic space groups, respectively [52]. Intriguingly, for the six space groups with Γ-enforced topology, observing a $\mu^{\mathrm{T}} = 2$ gap along high-symmetry paths in the BZ thus necessarily implies the existence of gap-closing nodal lines between bands 2 and 3 at generic momenta. We refer to this as a topological

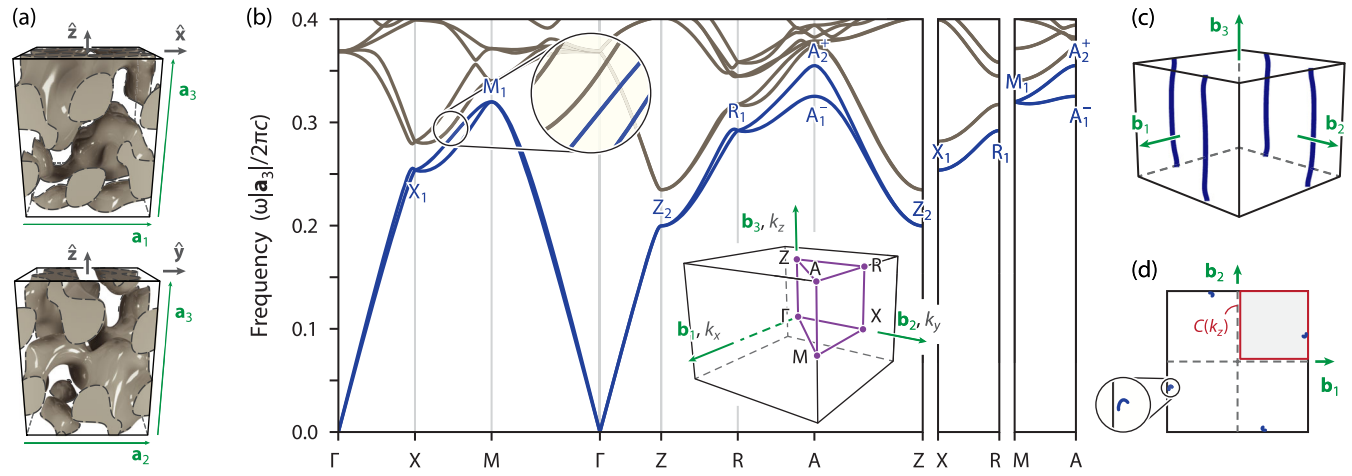

FIG. 3. Photonic topological nongap in space group 86 ($\mathrm{P4_2/n}$). (a) PhC unit cell and (b) associated band structure (along indicated BZ path) that realizes a minimum-connectivity ($\mu^{\mathrm{T}} = 2$) Γ-enforced topological solution in space group 86 (unit-cell parametrization in Supplemental Table S3 [37]; $\varepsilon = 16$ material in gray, embedded in vacuum with a filling fraction of 35%; $\mathbf{a}_i$ and $\mathbf{b}_i$, direct and reciprocal lattice vectors). (c) Four nodal lines connecting bands 2 and 3, running along k_z at generic (k_x, k_y). (d) Projection of nodal lines to the (k_x, k_y) plane and definition of a fixed-k_z loop $C(k_z)$, which encloses a quadrant of the (k_x, k_y) plane and a nodal line. Bands 1–4 do not touch on $C(k_z)$: The Berry phase of bands 2 and 3 (bands 1 and 4) around $C(k_z)$ is π (0), protecting an odd multiple of nodal lines in the interior of $C(k_z)$.

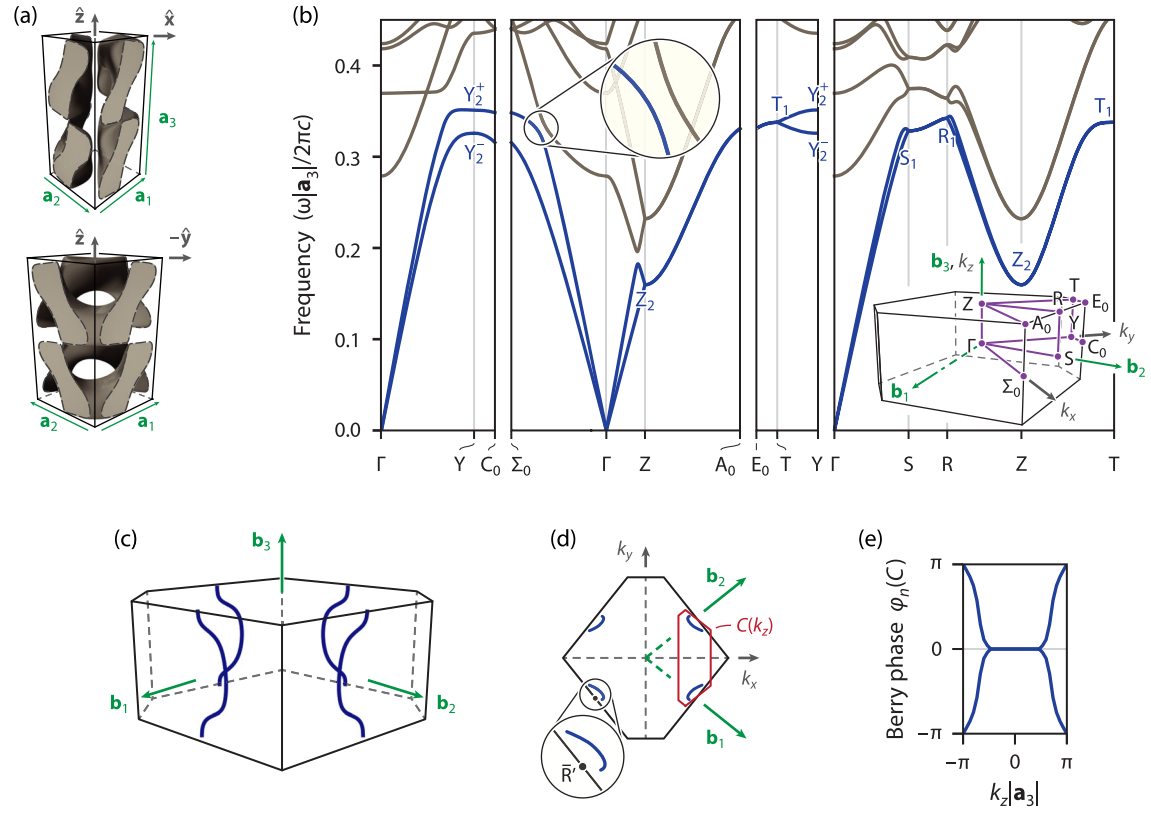

FIG. 4. Photonic topological nongap in space group 68 (Ccce) with $\mathbb{Z}_2$ monopole charge. (a) PhC unit cell and (b) associated band structure (along the indicated BZ path) that realizes a minimum-connectivity ($\mu^{\mathrm{T}} = 2$) Γ-enforced topological solution in space group 68 (unit-cell parametrization in Supplemental Table S4 [37]; $\varepsilon = 16$ material in gray, embedded in vacuum with a filling fraction of 35%; $\mathbf{a}_i$ and $\mathbf{b}_i$, direct and reciprocal primitive lattice vectors). (c) Nodal lines connecting bands 2 and 3 at generic momenta. (d) Projection of nodal lines to the (k_x, k_y) plane and definition of a fixed-k_z loop $C(k_z)$ that encloses a pair of nodal lines. (e) Non-Abelian Berry phases around $C(k_z)$ of bands 1 and 2 wind relatively when k_z ranges over its domain. The nodal lines are consequently protected by a $\mathbb{Z}_2$ monopole charge (in addition to a π-Berry phase).

"nongap": A high-symmetry gap that implies a gap closing. Nongaps demonstrate a new, topological constraint on photonic band connectivity beyond compatibility constraints. With this constraint accounted for, μ^{T} is increased from 2 to 4 for space groups 13, 48–50, 68, and 86 (Supplemental Sec. S8.A [37]).

We next demonstrate a concrete PhC with a topological nongap in space group 86 (generated by inversion -1 and screws $\{2_{001}|\frac{1}{2}\frac{1}{2}0\}$ and $\{4^{+}_{001}|0\frac{1}{2}\frac{1}{2}\}$). The $\mu^{\mathrm{T}} = 2$ compatibility-respecting solutions of space group 86 are $\mathbf{n}^{\mathrm{T}} = [(\blacksquare)^{2\mathrm{T}}, A_1^{\mp} + A_2^{\pm}, M_1, Z_2, R_1, X_1]$—with $(\blacksquare)^{2\mathrm{T}}$ indicating the singular Γ-point symmetry—with nontrivial index $\nu_1^{\mathrm{T}} = 1 \in \mathbb{Z}_2$. We perform a random search of PhCs spanned by symmetry-respecting Fourier-sum isosurfaces (Supplemental Sec. S3.D [37]), checking the symmetry vectors of their lowest two bands against $\mathbf{n}^{\mathrm{T}}$ to identify a realization [55]. Figures 3(a) and 3(b) show one such PhC realization: Its associated band structure shows a $\mu^{\mathrm{T}} = 2$ connectivity along the high-symmetry BZ paths. For regular TR-invariant bosonic bands in space group 86, a $\nu_1 = 1$ index protects a π-Berry phase in each quadrant of any k_z slice of the BZ (stabilized by the combination of TR and inversion symmetry), which in turn requires the existence of 4 (mod 8) nodal lines running along k_z [52]. Consistently, our PhC hosts four nodal lines between bands 2 and 3, each protected by a π-Berry phase in band 2 [Figs. 3(c) and 3(d)].

Unlike space group 86, the nodal lines of space groups 48–50 and 68 are protected not only by a π-Berry phase but also by a $\mathbb{Z}_2$ monopole charge (space group 13 may exhibit either type of protection) [52]. Figure 4 shows a PhC realization in space group 68 (generated by inversion -1, screws $\{2_{001}|\frac{1}{2}00\}$ and $\{2_{010}|00\frac{1}{2}\}$, and a C-centering translation $\{1|\frac{1}{2}\frac{1}{2}0\}$). The PhC realizes the sole $\mu^{\mathrm{T}} = 2$ compatibility-respecting solution, with symmetry vector $\mathbf{n}^{\mathrm{T}} = [(\blacksquare)^{2\mathrm{T}}, T_1, Y_2^{+} + Y_2^{-}, Z_2, R_1, S_1]$ and index $\nu_1^{\mathrm{T}} = 1 \in \mathbb{Z}_2$. The high-symmetry band structure thus exhibits a $\mu^{\mathrm{T}} = 2$ gap [Fig. 4(b)]—but there are nodal lines closing the gap at generic momenta [Fig. 4(c)]. For any loop enclosing a single nodal line, the summed Berry phase of bands 1 and 2 is π, as before. More interestingly, for a loop $C(k_z)$ enclosing a pair of nodal lines [Fig. 4(d)], bands 1 and 2 (and 3 and 4)

necessarily touch as k_z is wound over its domain [57]. Computing the non-Abelian Berry phases [58–60] of bands 1 and 2 over $C(k_z)$ while winding k_z, we observe a relatively winding Berry phase spectrum signaling an enclosed $\mathbb{Z}_2$ monopole charge [Fig. 4(e)] [61,62], consistent with the general predictions from topological band theory [52,63]. These $\mathbb{Z}_2$-charged nodal lines are protected against gapping by any TR- and inversion-preserving perturbations, just as the more conventional π-Berry phase nodal lines, but additionally, they can only be created and annihilated in pairs [62,64,65]. The impact of the distinct topological protections in space groups 86 and 68 could be detected experimentally since surface states extending from the projections of the nodal lines, e.g., at [001] facets, are single helicoid for π-Berry phase lines but double helicoid for $\mathbb{Z}_2$-charged lines [66,67].

We also search for Γ-enforced topology in the TR-broken setting, finding 32 space groups (Fig. 2, pink markers). However, since nontrivial TR-broken topology also includes gapped phases, this Γ-enforced topology does not necessarily correspond to topological nongaps. A prominent mechanism for breaking TR for photons involves applying a uniform magnetic field to magneto-optic PhC [68]. Among the identified candidates, only space groups 13, 85, 86, and 87 have symmetries compatible with a uniform magnetic field. Of these, only space groups 85 and 87 require TR breaking in order to exhibit Γ-enforced topology. By analyzing their solutions' symmetry, we find that the TR-broken minimum-connectivity ($\tilde{\mu}^{\mathrm{T}} = 2$) solutions of either case *cannot* be obtained by perturbatively applying TR breaking to their TR-invariant minimum-connectivity solutions. Instead, they require either large-amplitude TR breaking or fine-tuned accidental degeneracies (Supplemental Sec. S7 [37]).

Our discovery of topological nongaps is an interesting counterexample to the usual working assumption that a gap along the high-symmetry lines and edges of the BZ implies a full gap. Here, instead, the converse is guaranteed. While exceptions to the rule are well known [69,70], it is true that *most* band extrema occur at the BZ edge or along high-symmetry lines [69,71]. Our findings are consistent with this perspective since nodal lines are linear band degeneracies, not band extrema.

IV. DISCUSSION

Here, we have explicitly constructed the photonic minimum connectivity below the first gap by requiring consistency with compatibility relations and pinned symmetry content at $\omega = 0$. A natural question is whether every such connectivity can be realized with available optical materials. Space group 230 (Ia$\bar{3}$d), which, e.g., hosts the double-gyroid structure [72,73], provides an interesting counterexample: While we predict the possibility of a $\mu^{\mathrm{T}} = 8$ gap (Fig. 2), to the best of our knowledge, all previously observed gaps exhibit a higher connectivity [8,72]. This apparent discrepancy is caused by what we call a "dielectric obstruction"—a difficulty in bringing together the band symmetries required by a given solution because of material constraints. In more detail, every $\mu^{\mathrm{T}} = 8$ solution in Ia$\bar{3}$d requires a Γ_1^+ or Γ_1^- irrep or both (Supplemental Sec. S11.A [37]). These irreps, however, occur only in the very high-lying bands of PhCs in Ia$\bar{3}$d. To understand this, we consider the irreps of the empty-lattice structure (i.e., uniform ϵ): There, no $\Gamma_1^{\pm}$ features in the 38 lowest-frequency modes at Γ (Supplemental Sec. S10 [37]). To gradually transform the empty lattice to a hypothetical $\mu^{\mathrm{T}} = 8$ PhC then requires at least 38 band inversions at Γ—necessitating an extremely large dielectric contrast, likely outside the attainable range. Precisely where such dielectric obstructions arise is an interesting question, with implications for photonic topology and band engineering, in general.

Our construction relies explicitly on the use of a set of auxiliary apolar and longitudinal modes to circumvent the symmetry singularity at $\omega = 0$. This need arises because the transversality condition requires the discarding of one-third of all solutions to the Maxwell equations—the longitudinal modes—fracturing the symmetry content at $\omega = 0$. Unlike photons, phonons and acoustic waves allow both transverse and longitudinal polarizations; like photons, they intersect $\omega = 0$ at Γ but in a triply degenerate fashion [27]. Their symmetry content at $\omega = 0$ is consequently not singular, but it is still pinned by their long-wavelength plane-wave-like behavior. Phonons and acoustic waves are therefore subject to the apolar $\mathbf{n}_\Gamma^{\mathrm{1L+2T}}$ constraint in Eq. (3): The connected phononic solutions below the first gap are simply all the non-negative combinations of Hilbert vectors that each contribute to fulfilling this constraint. The minimum phononic connectivity below the first gap $\mu^{\mathrm{L+T}}$ (Fig. 5) can consequently be computed immediately with the tools already developed. The corresponding solutions are regular, and their (stable) topology can be evaluated directly from Eq. (5)—in fact, regularity also enables evaluation of fragile topology [74] (by checking non-negative integer expansion feasibility in the EBR basis; see Supplemental Sec. S2.F [37]). Doing so for every space group, we find no Γ-enforced topology in the TR-invariant setting but nine space groups with TR-broken Γ-enforced stable topology and three with fragile or mixed stable-fragile topology (Supplemental Sec. S11.C [37]). Such Γ-enforced topological phonons, or magnetic space-group analogues [75,76], may be realizable in ferroelectric materials. A related application is to the connectivity of bulk longitudinal plasmons of metals (associated with zeros of the longitudinal nonlocal dielectric function [77]) or to certain recently proposed perfect-metal metamaterials [78] (governed by the quasistatic Poisson equation), which, if wholly decoupled from transverse fields, are subject only to the $\mathbf{n}_\Gamma^{\mathrm{1L}}$ constraint in Eq. (3).

In this work, we provide explicit constructions of all minimum-connectivity solutions below the first gap in

FIG. 5. Minimum phononic and acoustic band connectivity below the first gap and associated Γ-enforced topology. Conventions are as in Fig. 2.

PhCs. Our approach exploits the existence of a Hilbert basis $\{\mathbf{h}_i\}$, consisting of all minimally connected bands, to very efficiently and exhaustively solve constrained connectivity problems. To apply this technique to the singular $\omega = 0$-connected transverse PhC bands, we introduce two auxiliary, regular problems associated with bands of apolar and longitudinal polarizations, whose difference corresponds to the physical transverse bands. Leveraging this decomposition further, we introduce a definition for the symmetry-identifiable topological indices of the singular PhC bands below the first gap in Eq. (6), thereby overcoming the key technical barrier to the application of a symmetry-based diagnosis of band topology to 3D PhCs [19]. By exhaustive computation of the topology of the minimum-connectivity solutions in every space group, we discover the existence of photonic topological nongaps—gaps in the

high-symmetry band structure whose existence implies necessary band closings, in the form of nodal lines, in the interior of the BZ—in space groups 13, 48–50, 68, and 86, providing proof-of-concept examples for the latter two.

The singular nature of the $\omega = 0$ bands is a uniquely photonic feature, arising as a direct result of the transverse polarization of photons. Beyond the problems considered here, the singularity's manifestations are at the core of several problems in electromagnetic theory, including, e.g., unique photonic considerations for $\mathbf{k} \cdot \mathbf{p}$ models [79] and long-standing obstacles to the construction of exponentially localized Wannier functions in 3D PhCs [80]. We expect the ideas introduced here to be useful also in these directions.

The software tools developed in this work are made available as open-source software implemented in the Julia programming language [33,81,82]. Functionality to compute general symmetry eigenvalues of PhC eigenstates was added to the MPB frequency-domain solver [56] as part of this work.

ACKNOWLEDGMENTS

We thank Ling Lu, Steven G. Johnson, and Robert-Jan Slager for stimulating discussions. This research is based upon work supported in part by the Air Force Office of Scientific Research under Grant No. FA9550-20-1-0115 and FA9550-21-1-0299, the U.S. Office of Naval Research (ONR) Multidisciplinary University Research Initiative (MURI) Grant No. N00014-20-1-2325 on Robust Photonic Materials with High-Order Topological Protection, and the U.S. Army Research Office through the Institute for Soldier Nanotechnologies at MIT under Collaborative Agreement No. W911NF-18-2-0048. The work of H. C. P. is partly supported by a Pappalardo Fellowship at MIT. The MIT SuperCloud and Lincoln Laboratory Supercomputing Center provided computing resources that contributed to the results reported in this work.

[1] J. D. Joannopoulos, S. G. Johnson, J. N. Winn, and R. D. Meade, *Photonic Crystals: Molding the Flow of Light*, 2nd ed. (Princeton University Press, Princeton, NJ, 2008).

[2] K. Sakoda, *Optical Properties of Photonic Crystals*, 2nd ed. (Springer, New York, 2004).

[3] Lord Rayleigh, *On the Maintenance of Vibrations by Forces of Double Frequency, and on the Propagation of Waves through a Medium Endowed with a Periodic Structure*, Philos. Mag. **24**, 145 (1887).

[4] Lord Rayleigh, *On the Remarkable Phenomenon of Crystalline Reflexion Described by Prof. Stokes*, Philos. Mag. **26**, 256 (1888).

[5] E. Yablonovitch, *Inhibited Spontaneous Emission in Solid-State Physics and Electronics*, Phys. Rev. Lett. **58**, 2059 (1987).

[6] S. John, *Strong Localization of Photons in Certain Disordered Dielectric Superlattices*, Phys. Rev. Lett. **58**, 2486 (1987).

[7] M. Maldovan, C. K. Ullal, W. C. Carter, and E. L. Thomas, *Exploring for 3D Photonic Bandgap Structures in the 11 f.c.c. Space Groups*, Nat. Mater. **2**, 664 (2003).

[8] R. K. Cersonsky, J. Antonaglia, B. D. Dice, and S. C. Glotzer, *The Diversity of Three-Dimensional Photonic Crystals*, Nat. Commun. **12**, 2543 (2021).

[9] M. Z. Hasan and C. L. Kane, *Colloquium: Topological Insulators*, Rev. Mod. Phys. **82**, 3045 (2010).

[10] B. A. Bernevig and T. L. Hughes, *Topological Insulators and Topological Superconductors* (Princeton University Press, Princeton, NJ, 2013).

[11] A. Bansil, H. Lin, and T. Das, *Colloquium: Topological Band Theory*, Rev. Mod. Phys. **88**, 021004 (2016).

[12] F. D. M. Haldane and S. Raghu, *Possible Realization of Directional Optical Waveguides in Photonic Crystals with Broken Time-Reversal Symmetry*, Phys. Rev. Lett. **100**, 013904 (2008).

[13] L. Lu, J. D. Joannopoulos, and M. Soljačić, *Topological Photonics*, Nat. Photonics **8**, 821 (2014).

[14] T. Ozawa, H. M. Price, A. Amo, N. Goldman, M. Hafezi, L. Lu, M. C. Rechtsman, D. Schuster, J. Simon, O. Zilberberg, and I. Carusotto, *Topological Photonics*, Rev. Mod. Phys. **91**, 015006 (2019).

[15] The perturbation of a dielectric profile $\boldsymbol{\varepsilon}(\mathbf{r})$ on an empty-lattice band of frequency $\omega_{n\mathbf{k}} = c|\mathbf{G} + \mathbf{k}|_n$ is dominated by the corresponding Fourier components of $\boldsymbol{\varepsilon}(\mathbf{r})$, i.e., of those $\boldsymbol{\varepsilon}_{\mathbf{G}'\mathbf{G}'}$ with $|\mathbf{G}' + \mathbf{k}| = |\mathbf{G} + \mathbf{k}|_n$. Fabrication constraints typically make $|\boldsymbol{\varepsilon}_{\mathbf{G}'\mathbf{G}'}|$ decrease rapidly with $|\mathbf{G}'|$, corresponding to reduced control of higher bands.

[16] H. Watanabe and L. Lu, *Space Group Theory of Photonic Bands*, Phys. Rev. Lett. **121**, 263903 (2018).

[17] L. Michel and J. Zak, *Connectivity of Energy Bands in Crystals*, Phys. Rev. B **59**, 5998 (1999).

[18] H. Watanabe, H. C. Po, M. P. Zaletel, and A. Vishwanath, *Filling-Enforced Gaplessness in Band Structures of the 230 Space Groups*, Phys. Rev. Lett. **117**, 096404 (2016).

[19] M. B. de Paz, M. G. Vergniory, D. Bercioux, A. García-Etxarri, and B. Bradlyn, *Engineering Fragile Topology in Photonic Crystals: Topological Quantum Chemistry of Light*, Phys. Rev. Research **1**, 032005(R) (2019).

[20] J. Kruthoff, J. de Boer, J. van Wezel, C. L. Kane, and R.-J. Slager, *Topological Classification of Crystalline Insulators through Band Structure Combinatorics*, Phys. Rev. X **7**, 041069 (2017).

[21] H. C. Po, A. Vishwanath, and H. Watanabe, *Symmetry-Based Indicators of Band Topology in the 230 Space Groups*, Nat. Commun. **8**, 50 (2017).

[22] B. Bradlyn, L. Elcoro, J. Cano, M. G. Vergniory, Z. Wang, C. Felser, M. I. Aroyo, and B. A. Bernevig, *Topological Quantum Chemistry*, Nature (London) **547**, 298 (2017).

[23] H. C. Po, H. Watanabe, M. P. Zaletel, and A. Vishwanath, *Filling-Enforced Quantum Band Insulators in Spin-Orbit Coupled Crystals*, Sci. Adv. **2**, e1501782 (2016).

[24] D. Wang, F. Tang, H. C. Po, A. Vishwanath, and X. Wan, $X\mathrm{Fe}_4\mathrm{Ge}_2$ $(X = \mathrm{Y}, \mathrm{Lu})$ *and* $\mathrm{Mn}_3\mathrm{Pt}$*: Filling-Enforced Magnetic Topological Metals*, Phys. Rev. B **101**, 115122 (2020).

[25] L. P. Bouckaert, R. Smoluchowski, and E. Wigner, *Theory of Brillouin Zones and Symmetry Properties of Wave Functions in Crystals*, Phys. Rev. **50**, 58 (1936).
[26] J. F. Cornwell, *Group Theory and Electronic Energy Bands in Solids* (North-Holland, Amsterdam, 1969).
[27] C. Kittel, *Quantum Theory of Solids*, 2nd ed. (John Wiley & Sons, New York, 1987).
[28] E. Kaxirax and J. D. Joannopoulos, *Quantum Theory of Materials* (Cambridge University Press, Cambridge, England, 2019).
[29] L. Michel and J. Zak, *Elementary Energy Bands in Crystals Are Connected*, Phys. Rep. **341**, 377 (2001).
[30] We use the data tables of ISO-IR to construct small irreps [31,32], accessed with the tooling developed in Ref. [33]. The associated irrep labels follow the CDML notation [34], consistently with, e.g., the Bilbao Crystallographic Server [35].
[31] H. T. Stokes, B. J. Campbell, and R. Cordes, *Tabulation of Irreducible Representations of the Crystallographic Space Groups and Their Superspace Extensions*, Acta Crystallogr. Sect. A **69**, 388 (2013).
[32] H. T. Stokes, D. M. Hatch, and B. J. Campbell, ISO-IR, ISOTROPY Software Suite (2013).
[33] Crystalline.jl (v0.4.17), https://github.com/thchr/Crystalline.jl.
[34] A. P. Cracknell, B. L. Davies, S. C. Miller, and W. F. Love, *Kronecker Product Tables. General Introduction and Tables of Irreducible Representations of Space Groups*, Vol. 1 (IFI/Plenum, New York, 1979).
[35] L. Elcoro, B. Bradlyn, Z. Wang, M. G. Vergniory, J. Cano, C. Felser, B. A. Bernevig, D. Orobengoa, G. Flor, and M. I. Aroyo, *Double Crystallographic Groups and Their Representations on the Bilbao Crystallographic Server*, J. Appl. Crystallogr. **50**, 1457 (2017).
[36] In the absence of magnetoelectric coupling, symmetry analysis can be performed interchangeably with either the electric **E** and dielectric **D** fields or the (pseudovectorial) magnetizing **H** and magnetic **B** fields (with inner products $\langle \mathbf{E}_{n\mathbf{k}} | \mathbf{D}_{n\mathbf{k}} \rangle$ or $\langle \mathbf{H}_{n\mathbf{k}} | \mathbf{B}_{n\mathbf{k}} \rangle$, respectively). With nonzero magnetoelectric coupling, i.e., for bi-(an)isotropic materials, the full inner product $\langle \mathbf{E}_{n\mathbf{k}} | \mathbf{D}_{n\mathbf{k}} \rangle + \langle \mathbf{H}_{n\mathbf{k}} | \mathbf{B}_{n\mathbf{k}} \rangle$ is necessary.
[37] See Supplemental Material at http://link.aps.org/supplemental/10.1103/PhysRevX.12.021066 for an extended summary of relevant theoretical background, a derivation of the Hilbert basis of compatibility-allowed bands, additional computational details, analysis of the unpinned symmetry of roto-inversions, proofs of invariance to the choice of longitudinal symmetry vector, comparison with the approach of Watanabe and Lu, discussion of time-reversal broken Γ-enforced topology and dielectric obstructions, enumeration of all regular band connectivities, and additional tables, including a full enumeration of all minimum-connectivity symmetry vectors and their topology.
[38] M. G. Vergniory, L. Elcoro, Z. Wang, J. Cano, C. Felser, M. I. Aroyo, B. A. Bernevig, and B. Bradlyn, *Graph Theory Data for Topological Quantum Chemistry*, Phys. Rev. E **96**, 023310 (2017).
[39] B. Bradlyn, L. Elcoro, M. G. Vergniory, J. Cano, Z. Wang, C. Felser, M. I. Aroyo, and B. A. Bernevig, *Band Connectivity for Topological Quantum Chemistry: Band Structures as a Graph Theory Problem*, Phys. Rev. B **97**, 035138 (2018).
[40] L. Elcoro, Z. Song, and B. A. Bernevig, *Application of Induction Procedure and Smith Decomposition in Calculation and Topological Classification of Electronic Band Structures in the 230 Space Groups*, Phys. Rev. B **102**, 035110 (2020).
[41] Z.-D. Song, L. Elcoro, Y.-F. Xu, N. Regnault, and B. A. Bernevig, *Fragile Phases as Affine Monoids: Classification and Material Examples*, Phys. Rev. X **10**, 031001 (2020).
[42] W. Bruns and J. Gubeladze, *Polytopes, Rings, and K-Theory* (Springer, New York, 2009).
[43] W. Bruns, B. Ichim, T. Römer, R. Sieg, and C. Söger, *Normaliz: Algorithms for Rational Cones and Affine Monoids*, https://normaliz.uos.de/.
[44] The 11 enantiomorphic pairs (chiral space groups related by a mirror) [45] must have identical global properties. More precisely then, μ^{T} is a property of the 219 affine space-group types.
[45] M. Nespolo, M. I. Aroyo, and B. Souvignier, *Crystallographic Shelves: Space-Group Hierarchy Explained*, J. Appl. Crystallogr. **51**, 1481 (2018).
[46] Incorporation of TR symmetry requires only swapping out EBRs and irreps for their TR-symmetric counterparts, i.e., physically real EBRs [22] and irreps (coreps) [47,48].
[47] C. Herring, *Effect of Time-Reversal Symmetry on Energy Bands of Crystals*, Phys. Rev. **52**, 361 (1937).
[48] C. J. Bradley and A. P. Cracknell, *The Mathematical Theory of Symmetry in Solids* (Clarendon Press, Oxford, 1972).
[49] *International Tables for Crystallography Volume A: Space-group Symmetry*, edited by M. I. Aroyo, 6th ed. (Wiley, New York, 2016).
[50] As an example, space group 85 (P4/n) is a key group for space group 126 (P4/nnc): While P4/n is generated by inversion -1 and a fourfold screw $\{4^{+}_{001}|\frac{1}{2}00\}$ and has $\mu^{\mathrm{T}} = 2$, P4/nnc contains an additional twofold screw (or, equivalently, a glide) axis among its generators, e.g., $\{2_{100}|\frac{1}{2}00\}$, and has $\mu^{\mathrm{T}} = 4$.
[51] We note a single disagreement with Ref. [8], which reported a PhC with a 0.1% gap between bands 2 and 3 in space group 224, inconsistently with $\mu^{\mathrm{T}} = 4$ found here. This gap appears to be spurious and is likely due to numerical symmetry breaking.
[52] Z. Song, T. Zhang, and C. Fang, *Diagnosis for Nonmagnetic Topological Semimetals in the Absence of Spin-Orbital Coupling*, Phys. Rev. X **8**, 031069 (2018).
[53] F. Tang, H. C. Po, A. Vishwanath, and X. Wan, *Efficient Topological Materials Discovery Using Symmetry Indicators*, Nat. Phys. **15**, 470 (2019).
[54] As a complementary perspective, Eq. (5) is more generally applicable not only to elements of the monoid $\{\mathrm{BS}\}$ but also to the free Abelian group $\{\overline{\mathrm{BS}}\}$ whose elements include solutions to the compatibility relations with negative content (Supplemental Sec. S2.C [37]). Notably, while $\mathbf{n}^{\mathrm{T}}$, in general, does not belong to $\{\mathrm{BS}\}$, it does belong to $\{\overline{\mathrm{BS}}\}$.
[55] Our calculations use the MPB frequency-domain solver [56].
[56] S. G. Johnson and J. D. Joannopoulos, *Block-Iterative Frequency-Domain Methods for Maxwell's Equations in a Planewave Basis*, Opt. Express **8**, 173 (2001).

[57] The loop $C(k_z)$ must intersect the $\mathbf{k}$ line $A = \alpha\mathbf{b}_1 + \alpha\mathbf{b}_2 + \frac{1}{2}\mathbf{b}_3$ (primitive reciprocal lattice vectors $\mathbf{b}_i$) whose only irrep is 2D.
[58] F. Wilczek and A. Zee, *Appearance of Gauge Structure in Simple Dynamical Systems*, Phys. Rev. Lett. **52**, 2111 (1984).
[59] A. A. Soluyanov, Ph.D. thesis, Rutgers, The State University of New Jersey (2012).
[60] D. Vanderbilt, *Berry Phases in Electronic Structure Theory* (Cambridge University Press, Cambridge, England, 2018).
[61] R. Yu, X. L. Qi, A. Bernevig, Z. Fang, and X. Dai, *Equivalent Expression of $\mathbb{Z}_2$ Topological Invariant for Band Insulators Using the Non-Abelian Berry Connection*, Phys. Rev. B **84**, 075119 (2011).
[62] J. Ahn, D. Kim, Y. Kim, and B.-J. Yang, *Band Topology and Linking Structure of Nodal Line Semimetals with Z_2 Monopole Charges*, Phys. Rev. Lett. **121**, 106403 (2018).
[63] There is an inconsequential cosmetic difference between the nodal lines in Fig. 4(c) and those predicted in Ref. [52]: We observe paired nodal lines rather than loops; the former can be obtained from the latter by merging across the $k_z = 0$ plane.
[64] C. Fang, Y. Chen, H.-Y. Kee, and L. Fu, *Topological Nodal Line Semimetals with and without Spin-Orbital Coupling*, Phys. Rev. B **92**, 081201(R) (2015).
[65] Y. Kim, B. J. Wieder, C. L. Kane, and A. M. Rappe, *Dirac Line Nodes in Inversion-Symmetric Crystals*, Phys. Rev. Lett. **115**, 036806 (2015).
[66] C. Fang, L. Lu, J. Liu, and L. Fu, *Topological Semimetals with Helicoid Surface States*, Nat. Phys. **12**, 936 (2016).
[67] H. Cheng, Y. Sha, R. Liu, C. Fang, and L. Lu, *Discovering Topological Surface States of Dirac Points*, Phys. Rev. Lett. **124**, 104301 (2020).
[68] Z. Wang, Y. Chong, J. D. Joannopoulos, and M. Soljačić, *Observation of Unidirectional Backscattering-Immune Topological Electromagnetic States*, Nature (London) **461**, 772 (2009).
[69] J. M. Harrison, P. Kuchment, A. Sobolev, and B. Winn, *On Occurrence of Spectral Edges for Periodic Operators Inside the Brillouin Zone*, J. Phys. A **40**, 7597 (2007).
[70] R. V. Craster, T. Antonakakis, M. Makwana, and S. Guenneau, *Dangers of Using the Edges of the Brillouin Zone*, Phys. Rev. B **86**, 115130 (2012).
[71] F. Maurin, C. Claeys, E. Deckers, and W. Desmet, *Probability that a Band-Gap Extremum Is Located on the Irreducible Brillouin-Zone Contour for the 17 Different Plane Crystallographic Lattices*, Int. J. Solids Struct. **135**, 26 (2018).
[72] L. Lu, L. Fu, J. D. Joannopoulos, and M. Soljačić, *Weyl Points and Line Nodes in Gyroid Photonic Crystals*, Nat. Photonics **7**, 294 (2013).
[73] L. Lu, Z. Wang, D. Ye, L. Ran, L. Fu, J. D. Joannopoulos, and M. Soljačić, *Experimental Observation of Weyl Points*, Science **349**, 622 (2015).
[74] H. C. Po, H. Watanabe, and A. Vishwanath, *Fragile Topology and Wannier Obstructions*, Phys. Rev. Lett. **121**, 126402 (2018).
[75] H. Watanabe, H. C. Po, and A. Vishwanath, *Structure and Topology of Band Structures in the 1651 Magnetic Space Groups*, Sci. Adv. **4**, eaat8685 (2018).
[76] L. Elcoro, B. J. Wieder, Z. Song, Y. Xu, B. Bradlyn, and B. A. Bernevig, *Magnetic Topological Quantum Chemistry*, Nat. Commun. **12**, 5965 (2021).
[77] D. Pines and D. Bohm, *A Collective Description of Electron Interactions: II. Collective vs Individual Particle Aspects of the Interactions*, Phys. Rev. **85**, 338 (1952).
[78] W.-J. Chen, B. Hou, Z.-Q. Zhang, J. B. Pendry, and C.-T. Chan, *Metamaterials with Index Ellipsoids at Arbitrary $\mathbf{k}$-points*, Nat. Commun. **9**, 1 (2018).
[79] J. E. Sipe, *Vector $k \cdot p$ Approach for Photonic Band Structures*, Phys. Rev. E **62**, 5672 (2000).
[80] C. Wolff, P. Mack, and K. Busch, *Generation of Wannier Functions for Photonic Crystals*, Phys. Rev. B **88**, 075201 (2013).
[81] SymmetryBases.jl (v0.4.0), https://github.com/thchr/SymmetryBases.jl.
[82] PhotonicBandConnectivity.jl (v0.3.0), https://github.com/thchr/PhotonicBandConnectivity.jl.